Supplemental Materials

Molecular Biology of the Cell

Varadarajan et al.

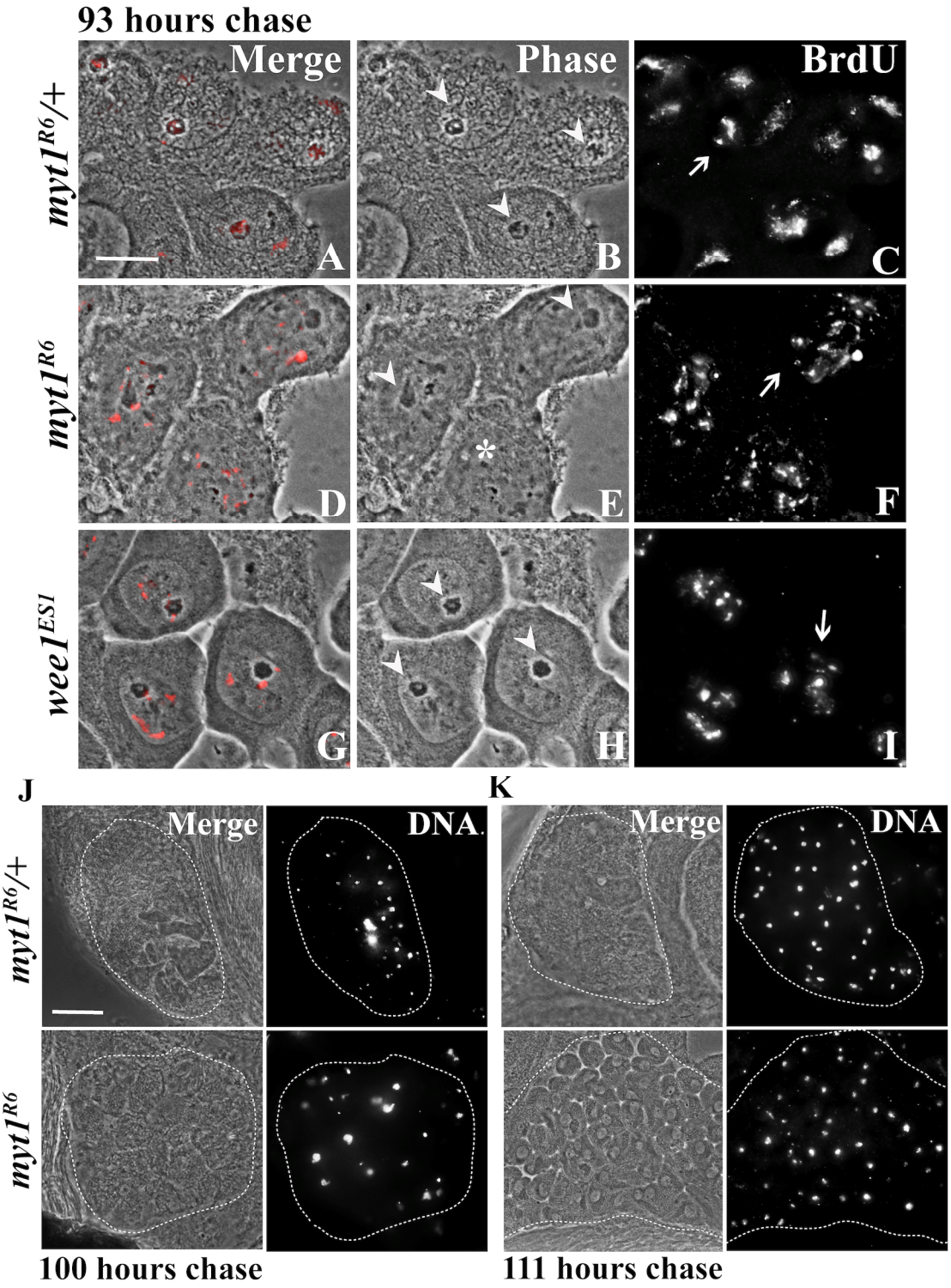

Figure S1: Timing of pre-meiotic G2 phase arrest is unperturbed in *myt1* and *wee1* spermatocytes (A-I) Examples of BrdU-labeled spermatocytes examined at

the indicated times post-chase. In panels J-K, the BrdU (red) channel was removed for clarity. (A-C) At 93±2 hour post-chase, BrdU-labeled *myt1*/+ spermatocytes are at stage S5 with intact nucleoli (arrowhead, B) and characteristic chromosome organization (arrow). (D-F) In *myt1* mutants fixed at 93±2 hour post-chase, we could observe cysts with mature spermatocytes having either an intact nucleolus (arrowhead) or no observable nucleolus (asterisk). These variations in nucleolar appearance (E) did not correlate with obvious differences in chromosome organization within three cells of what appears to be an intact *myt1* mutant cyst (F), however the chromatin appeared more dispersed than comparably aged *myt1*/+ controls (compare C with F). Chromatin defects were also reported in proliferating mitotic cells of *myt1* mutant imaginal discs by Jin *et al.*, 2008. (G-I) BrdU-labeled *wee1* mutants fixed at 93 hr post-chase appeared identical to the controls. (J) At 100 hr post-chase, BrdU-labeled *myt1*/+ control cysts contained more than 16 cells (~ 32 cells, n=2 cysts), indicating completion of Meiosis I. (K) At 111 hr post-chase, all of the BrdU labeled control cysts contained more than 32 cells (~ 64 cells, n=2 cysts), indicating completion of Meiosis II. BrdU-labeled *myt1* cysts contained similar numbers of cells at the 100 and 111 hr post-chase time points (n=2 cysts). Scale bar -10 μm.

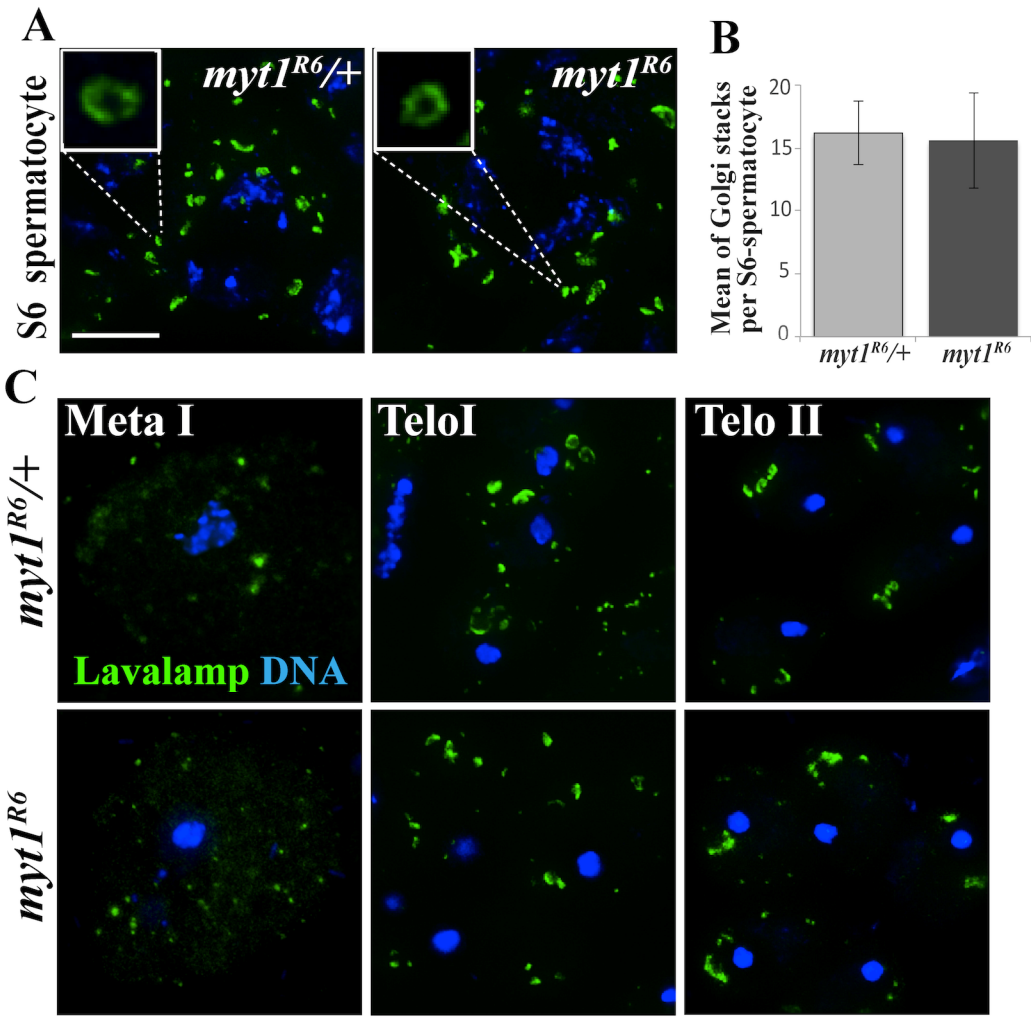

Figure S2: Golgi organization appears normal in *myt1* mutants during Meiosis I and II. (A) Stage S6 spermatocytes immunolabeled for Lava lamp (green) to mark the peripheral Golgi. Captured Z-stacks of these images were merged and deconvolved, showing that similar numbers of individual "ring shaped" Golgi stacks were present in the *myt1/+* and *myt1* mutant spermatocytes (see insets, showing a single plane). (B) Graph showing quantification of the number of Golgi stacks per stage S6 spermatocyte. These numbers were calculated by analyzing deconvolved Z-stacks so we could be confident we were counting individual Golgi stacks (n=74 for *myt1/+;* n=85 for *myt1*). Error bar indicates the standard deviation of the mean. (C) Spermatocytes labeled for

Lva, showing meiotic Golgi disassembly and reassembly after exit from Meiosis I and II. Scale bar-10 μm.

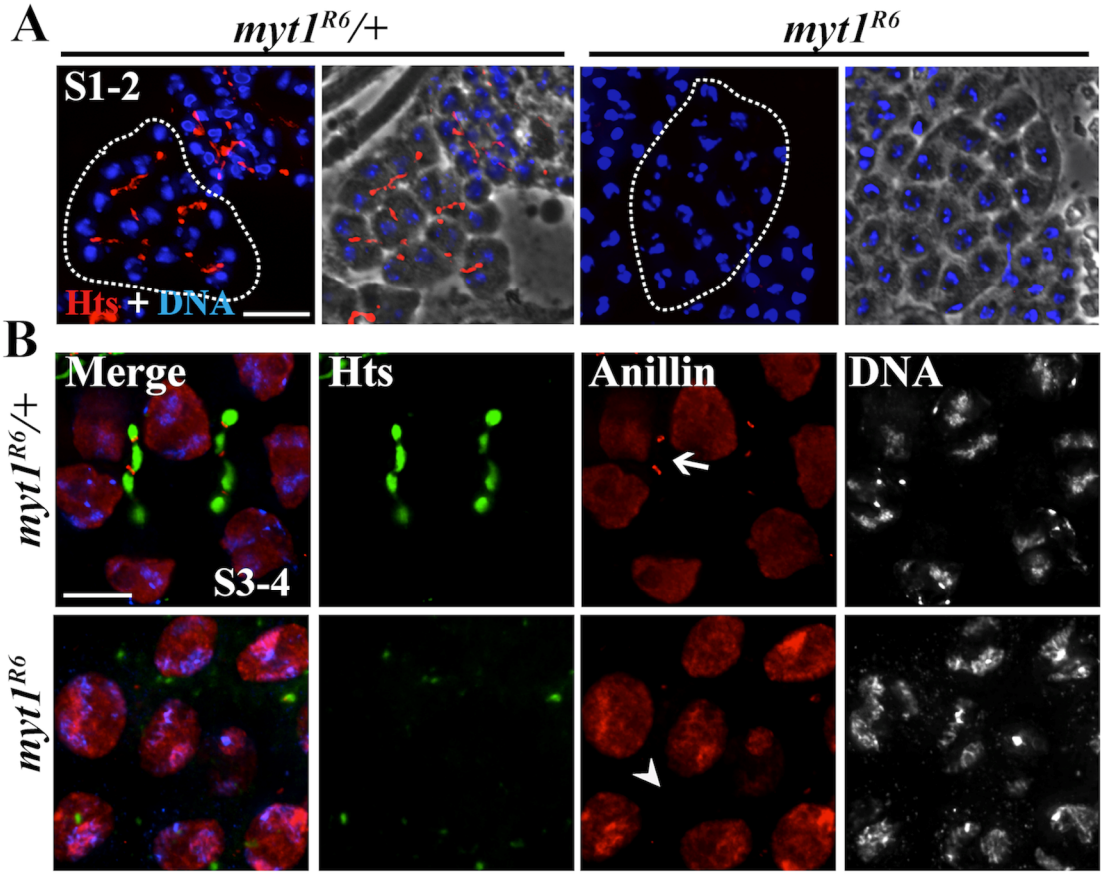

Figure S3: Loss of Myt1 activity results in fusome defects as early as Stage S1-2. (A) Early stage S1-2 spermatocytes identified by cell size and small, intensely labeled nuclei (blue) were immunolabeled for Hts to mark fusomes (red). Fusomes can be seen interconnecting the *myt1/+* spermatocytes in a single cyst (circled). In *myt1* mutant cysts, the fusomes were undetectable. Scale bar -10 μm. (B) Stage S3-4 spermatocytes immunolabeled for Hts (green) to mark fusomes, Anillin (red, arrow) to mark ring canals and labeled for DNA. The fusomes were absent and ring canals difficult to detect

(arrowhead) at this stage in the *myt1* mutants, compared to the controls. Scale bar -10 μm.

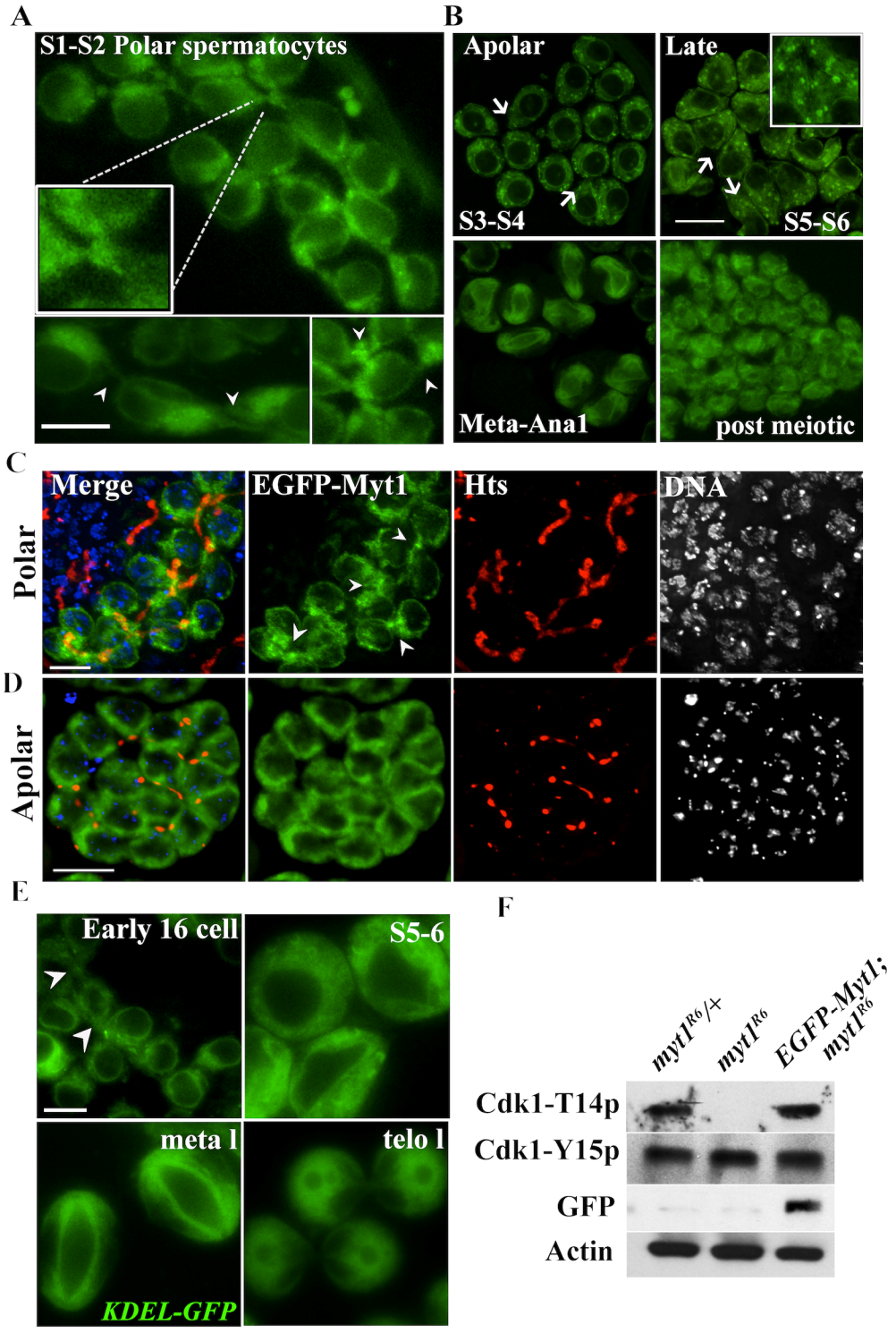

Figure S4: Characterization of *EGFP-Myt1* localization and biochemical activity. Myt1 is a membrane-associated protein that localizes to ER and Golgi membranes. Since antibodies were not available for studying *Drosophila* Myt1 localization we synthesized transgenic strains (see Materials and Methods) for Gal4-inducible UASp-*EGFP-Myt1* and β2-tubulin (*tv3*)-driven expression of *GFP-Myt1*. (A, B) Live imaging of transgenic EGFP-Myt1 at the indicated stages of development (A) In polar spermatocytes (stage S1-2), EGFP-Myt1 is primarily cytoplasmic and enriched at inter-cellular junctions (inset, arrowhead). Scale bar - 10 μm. (B) In apolar spermatocytes (stage S3-4), GFP-Myt1 was cytoplasmic but no longer detectable at inter-cellular junctions (arrows). In mature (stage S5-6) spermatocytes the inset shows enriched GFP-Myt1 labeling of structures, resembling Golgi stacks. During metaphase I, GFP-Myt1 labeling appeared to envelop the meiotic spindle. In post-meiotic cells, GFP-Myt1 diffusely labeled cytoplasmic structures. Scale bar - 20 μm. (C) Fixed polar and apolar spermatocytes expressing EGFP-Myt1 (green) were co-labeled with Hts (red) and DNA (blue). In polar (S1-2) stages the EGFP-Myt1 signal partially co-localized with Hts-labeled fusome bridges (arrowheads). Scale bar-10 μm (D) In fixed, apolar spermatocytes (S3-4), EGFP-Myt1 co-localization with Hts-labeling was reduced or absent. Scale bar - 16 μm. The ring-shaped structures observable at this stage in live spermatocytes (Fig S4B) were not observable in fixed cells, suggesting they were sensitive to the fixation conditions used for Hts-labeling. (E) Live imaging of spermatocytes expressing EGFP-KDEL as a reporter for the endoplasmic reticulum (Snapp et al., 2004), at different stages of development. Note that this ER reporter marks intercellular bridges in early (S1-S2) spermatocyte and a meiotic sheath in metaphase I, similar to live imaging of EGFP-Myt1

(Figure S4A and S4B). Scale bar-10 μm. (F) Western blotting of whole testes extracts from young adult flies of the indicated genotypes. The blots were probed sequentially with phospho-specific antibodies against endogenous Cdk1-T14p and Cdk1-Y15p, with actin as a loading control. The molecular weight of endogenous Cdk1 is approximately 34 kDa. Anti-GFP antibodies were used to detect EGFP-Myt1 expression in a *myt1* mutant background. The molecular weight of EGFP-Myt1 is 92 kDa and Actin is 47 kDa. In the *myt1*/+ controls, both phospho-inhibited isoforms were observed for endogenous Cdk1. The Cdk1-T14p isoform was absent in the *myt1* mutant sample, but restored by expression of EGFP-Myt1. The presence of the Cdk1-Y15p isoform was expected because Wee1 was previously shown to be functionally redundant for phosphorylation of this residue (Jin et al., 2008; Kao et al., 2015).

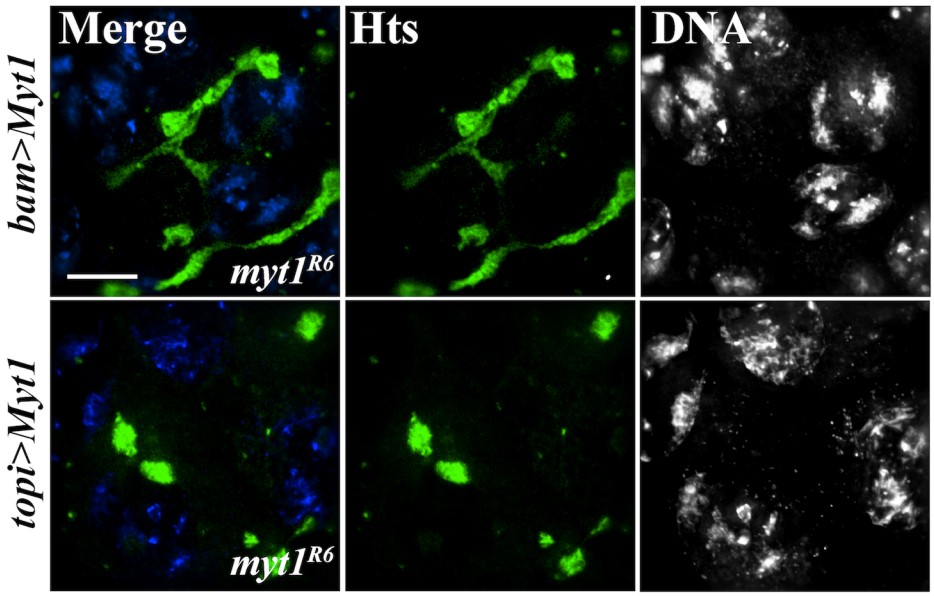

Figure S5: EGFP-tagged Myt1 expressed in early spermatocytes rescues *myt1* mutant defects

Stage S3-4 *myt1* mutant spermatocytes were staged by DNA labeling. In fixed *myt1* spermatocytes expressing *bam-Gal4 >EGFP-Myt1* we observed 100% normal fusomes (n=28 intact cysts) of Hts-labeled fusomes (green), whereas *topi-Gal4 >EGFP-Myt1* expression only partially rescued this defect (94%, partial and 6% no fusomes, n=31 intact cysts). Scale bar -10 μm.

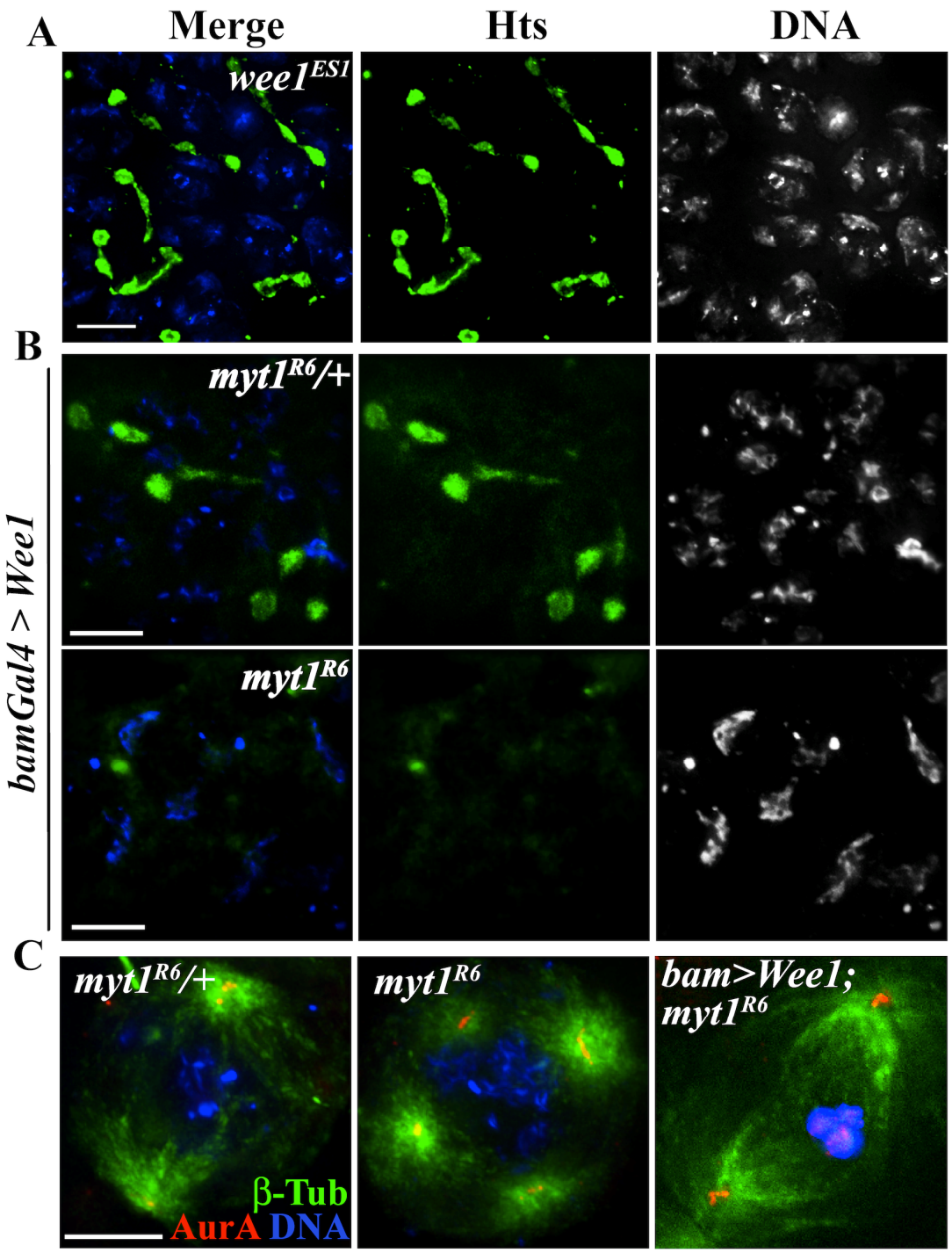

Figure S6: Ectopic Wee1 rescues *myt1* mutant centrosome defects but not fusome integrity

(A) Hts-labeled fusomes appeared normal in *wee*^{ES1} mutants and (B) *bam-Gal4* driven expression of *UASp-Wee1* alone, but did not rescue the *myt1* mutant fusome defect (n=28 intact cysts). (C) Expression of *bam>UASp-Wee1* restored bipolar MI meiotic spindles in *myt1* mutant spermatocytes (n=94 intact cysts) that were immunolabeled for β–Tubulin (green), AuroraA-T288p (red) and DNA (blue). Scale bar -10 μm.

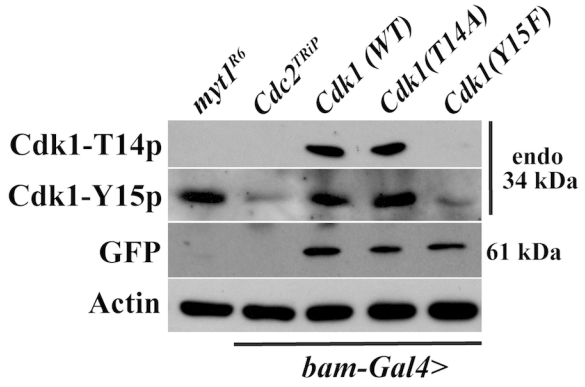

Figure S7: *bam> Cdk1 (Y15F)* expression in spermatocytes activates endogenous Cdk1

Western blot showing the biochemical effects of transgenic Cdk1(Y15F) expression. Testes extracts from young adults of the indicated genotypes were probed sequentially with phospho-specific antibodies to detect endogenous (34 kD) Cdk1-T14p and Cdk1-Y15p, with actin as a loading control. Anti-GFP antibodies were used to detect the Cdk1:VFP transgenes (61 kD). The Cdk1-T14p isoform was absent in the *myt1* controls, as expected (lane1). Depletion of endogenous Cdk1 (Cdc2) by *bamGal4* >Cdc2^{TRiP} expression reduced the signal for Cdk1-T14p and Y15p phospho-isoforms (lane 2). Cdk1(WT)-VFP, Cdk1(T14A)-VFP and Cdk1(Y15F)-VFP were individually expressed in early spermatocytes using *bam-Gal4* driver. Endogenous Cdk1 (34 kDa) T14p and Y15p phospho-isoforms appeared unaffected in the *bam>Cdk1(WT)*-VFP and

bam>Cdk1(T14A)- VFP extracts, however these Cdk1 inhibitory phospho-isoforms were markedly reduced in *bam>Cdk1(Y15F)* extracts, indicating that expression of Cdk1(Y15F) activated endogenous Cdk1.

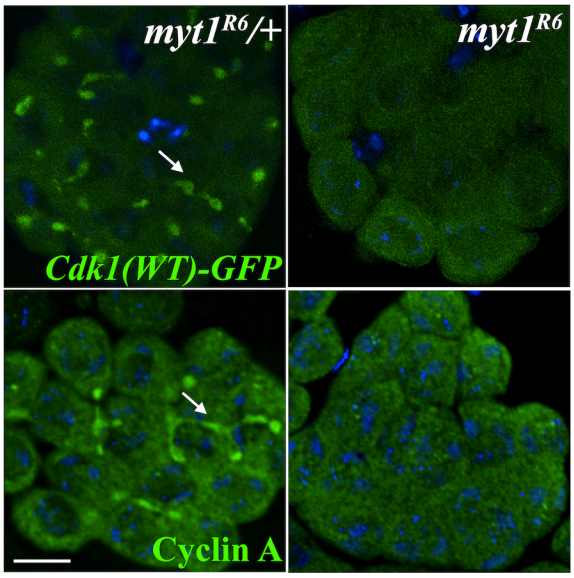

Figure S8: Cdk1(WT)-GFP and Cyclin A localization to fusomes was undetectable in *myt1* mutants. (Top row) Expression of Cdk1(WT)-GFP, showing fusome localization in a *myt1*/+ background (arrows) that was undetectable in *myt1* mutants. (Bottom row) When spermatocytes were immunolabeled for Cyclin A, the fusome localization observed in *myt1*/+ control spermatocytes was undetectable in *myt1* mutants. Scale bar - 32 μm.

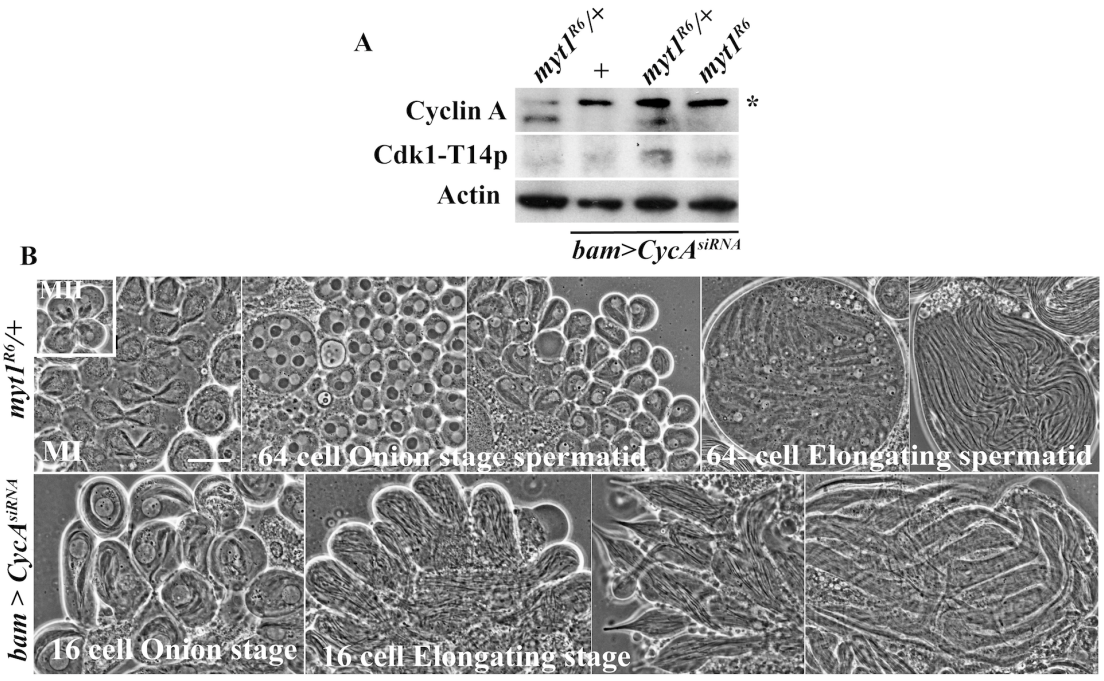

Figure S9: CyclinA depletion by *bam>Cyclin A*^{siRNA} prevents MI progression.

(A) Western blot probed sequentially with Cyclin A, Cdk1-T14p and actin antibodies. Cyclin A labeling detected a doublet (also reported by Lehner and O'Farrell, 1989). The top band corresponding to an undetermined 70 kDa protein was not affected by *Cyclin A*^{siRNA} whereas a lower ~56 kDa band representing endogenous Cyclin A was missing. There was no effect on T14 inhibitory phosphorylation of endogenous Cdk1 by *Cyclin A*^{siRNA} depletion. (B) Phase contrast images of control and *bam>CycA*^{siRNA} spermatocytes and spermatids, illustrating how depletion of Cyclin A affected different stages of meiosis. In *myt1/+* controls, progression through MI and MII was followed by spermatid remodeling in post-meiotic 64-cell cysts. When Cyclin A was depleted by *bam >Cyclin A*^{siRNA} expression the 16-cell spermatocytes do not finish MI but arrested in prometaphase-I before undergoing aberrant morphological changes associated with spermatid differentiation. Scale bar-10 μm.

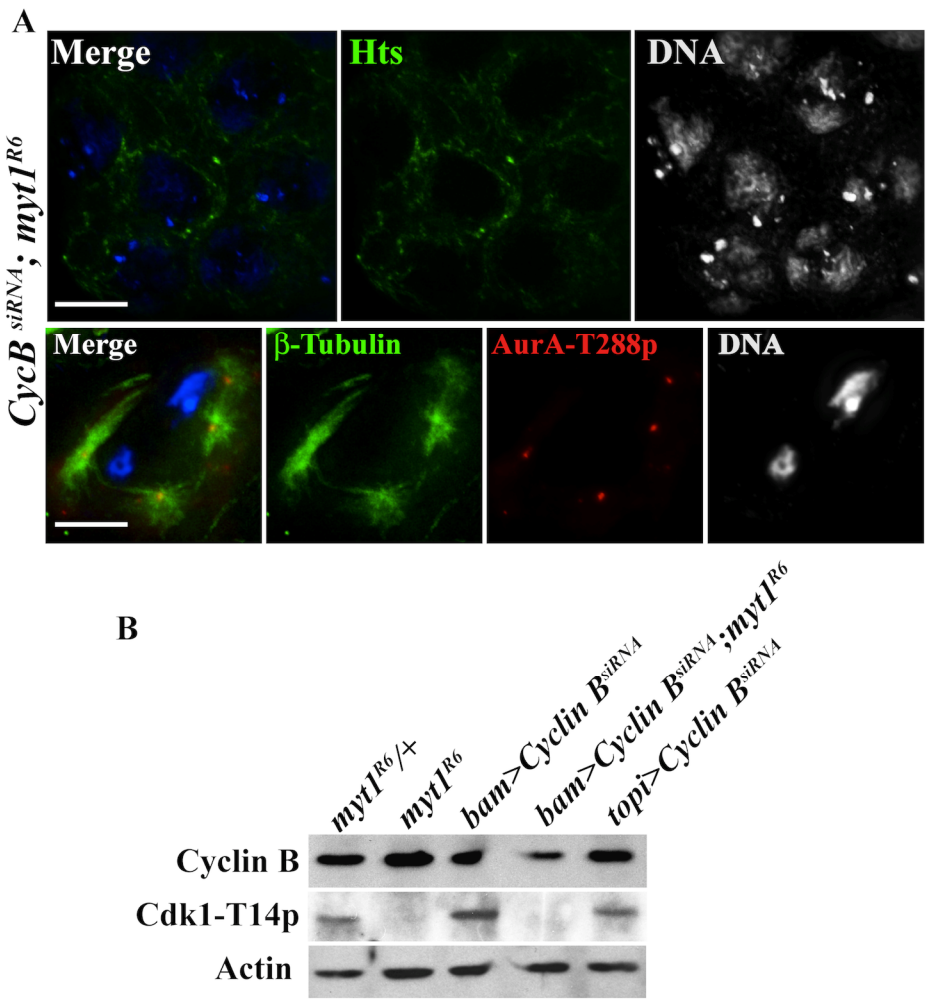

Figure S10: *myt1* mutant fusome and centriole defects are not rescued by *bam>Cyclin B^{siRNA}*.

(A) Fusomes were undetectable by Hts labeling (green) in *myt1* mutant spermatocytes expressing *bam>Cyclin B^{siRNA}*. (B) Multipolar *myt1* mutant meiotic spindles labeled with β–Tubulin (green) and AuroraA-T288 (red) were also not rescued by *bam>CycB^{siRNA}* expression. Scale bar -10 μm. (B) Western blot probed sequentially for Cyclin B, Cdk1-T14p and actin as a loading control. Endogenous Cyclin B corresponding to a 52 kDa band was not noticeably affected by *CycB^{siRNA}* expression in the different genotypes shown.

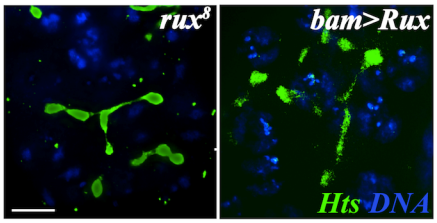

Figure S11: Controls for effects of loss of Rux function or ectopic *Rux* expression.

Hts-labeled fusome structures appeared normal in both *rux*^{8} mutant and *bam* driven *UAS-Rux* expression in spermatocytes. Scale bar -10 μm.